

# Principles of Cerebral Perfusion Imaging by Bolus Tracking

Leif Østergaard, MD, PhD\*

The principles of cerebral perfusion imaging by the method of dynamic susceptibility contrast magnetic resonance imaging (DSC-MRI) (bolus tracking) are described. The MRI signals underlying DSC-MRI are discussed. Tracer kinetics procedures are defined to calculate images of cerebral blood volume (CBV), cerebral blood flow (CBF), and mean transit time (MTT). Two general categories of numerical procedures are reviewed for deriving CBF from the residue function. Procedures that involve deconvolution, such as Fourier deconvolution or singular value decomposition (SVD), are classified as model-independent methods because they do not require a model of the microvascular hemodynamics. Those methods in principle also yield a measure of the tissue impulse response function and the residue function, from which microvascular hemodynamics can be characterized. The second category of methods is the model-dependent methods, which use models of tracer transport and retention in the microvasculature. These methods do not yield independent measures of the residue function and may introduce bias when the physiology does not follow the model. Statistical methods are sometimes used, which involve treating the residue function as a deconvolution kernel and optimizing (fitting) the kernel from the experimental data using procedures such as maximum likelihood. Finally, other hemodynamic indices that can be measured from DSC-MRI data are described.

**Key Words:** dynamic susceptibility contrast; cerebral perfusion imaging; perfusion methodology; deconvolution; cerebral blood flow

**J. Magn. Reson. Imaging 2005;22:710–717.**  
© 2005 Wiley-Liss, Inc.

PERFUSION MEASUREMENTS by dynamic susceptibility contrast magnetic resonance imaging (DSC-MRI) utilize very rapid imaging (most commonly echo planar imaging (EPI)) to capture the first pass of intravenously injected paramagnetic contrast agent—hence the term

bolus tracking. By kinetic analysis of these data, hemodynamic indices, namely, cerebral blood flow (CBF), cerebral blood volume (CBV), and mean transit time (MTT), can be derived. This paper reviews the principles of perfusion imaging using the DSC-MRI bolus tracking method. Other approaches to measure perfusion with MRI, such as arterial spin labeling (ASL), are reviewed and discussed in other papers in this journal issue, and both methods are reviewed in Calamante et al (1).

## THEORY

To derive hemodynamic parameters from dynamic MR images by tracer kinetic analysis, the contrast agent concentrations in various tissue compartments must be known. For a given pulse sequence (e.g., spin echo (SE) or gradient echo (GE) EPI) the relation between observed signal changes during the contrast agent bolus passage and the corresponding concentration must be known in detail.

## SUSCEPTIBILITY CONTRAST

Bolus tracking is commonly carried out using DSC imaging, tracking the passage of a rapidly injected paramagnetic gadolinium (Gd)-based chelate by a  $T_2$ - (SE) or  $T_2^*$ - (GE) weighted sequence (often EPI). In the brain, the first-pass extraction of contrast agent is zero when the blood-brain barrier is reasonably intact, and the intravascular compartmentalization of contrast agent creates strong, microscopic susceptibility gradients. These microscopic gradients cause dephasing of spins as the spins diffuse among these gradients, which results in signal loss in  $T_2$ - and  $T_2^*$ -weighted images, as described by Villringer et al (2) in 1998. Whereas pulse sequences *without* full refocusing of static field inhomogeneities (GEs) will experience a general signal loss due to the presence of microscopic field perturbations in the vessels, the signal loss is far less for pulse sequences where dephasing is partially refocused (SEs). For the SE sequence, signal loss is observed at long echo times, during which water diffuses through areas of different magnetic fields. The signal loss is most pronounced when most spins in or near the contrast filled vessel have the opportunity to diffuse across the susceptibility gradient at the vessel walls during the course of the experiment, i.e., during the echo time TE. The diffusion-related sig-

Department of Neuroradiology, Center for Functionally Integrative Neuroscience (CFIN), Aarhus University Hospital, Århus, Denmark.

Contract grant sponsor: Danish National Research Foundation; Contract grant sponsor: Danish Medical Research Council.

\*Address reprint requests to: L.Ø., Department of Neuroradiology, Center for Functionally Integrative Neuroscience (CFIN), Building 30, Århus University Hospital, Nørrebrogade 44, 8000 Århus C, Denmark.  
E-mail: leif@pet.auh.dk

Received March 15, 2005; Accepted September 20, 2005.

DOI 10.1002/jmri.20460

Published online 31 October 2005 in Wiley InterScience (www.interscience.wiley.com).

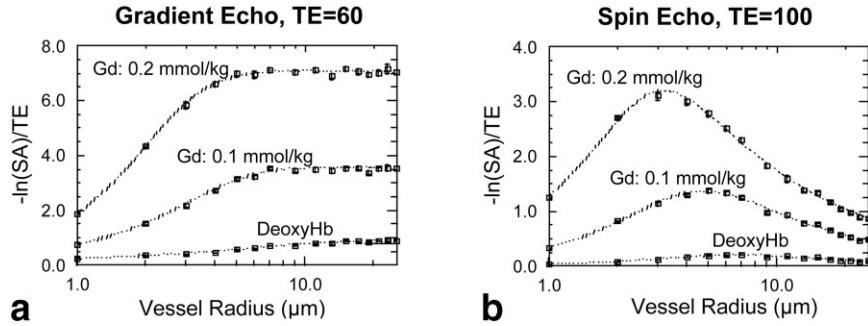


**Figure 1.** Change in transverse relaxation rate as a function of vessel size caused by typical Gd dosages and deoxyhemoglobin for SE (a) and GE (b) sequences at typical TE values. The Gd dosages were single and double dose (0.1 and 0.2 mmol/kg, respectively). Note the microvascular sensitivity of the SE sequence (in the range of capillary diameters), while GE is sensitive to all vessel sizes. The change in transverse relaxation rate is given by  $-\ln(SA)/TE$ , where SA is the signal attenuation factor given by the ratio of the postcontrast vs. precontrast signal intensity.

nal loss is hence a complex function of TE, the density of the distribution of vessel sizes, and the concentration and magnetic properties of the contrast agent. Weisskoff, Boxerman, and co-workers (3–5) performed a detailed analysis of these effects using Monte Carlo modeling as well as experimental data. They found that SE measurements are mainly sensitive to vessel sizes comparable to the water diffusion length during the time of echo ( $\sim 10 \mu\text{m}$ ), whereas GE measurements are equally sensitive to all vessel sizes (Fig. 1). Experimentally and clinically, this sensitivity difference requires that twice the amount of contrast agent be injected if imaging is performed using SE-EPI, relative to imaging with GE-EPI (as used in Fig. 2). Typically, a double dose of standard Gd chelate (0.2 mmol/kg) is injected for SE-EPI, while a single dose (0.1 mmol/kg) is generally injected in GE-EPI, as in Fig. 2. In return for this, the SE signal theoretically yields preferential sensitivity in detecting changes in small vessel density. Preliminary studies suggest that, in the brain, the microvascular CBV visible by SE-EPI is roughly 45% of the total CBV, as observed by positron emission tomography (PET) (6) or GE-EPI (7). As important, the study in Simonsen et al (7) found that an approximate linear relationship exists between tissue contrast agent concentration and change in  $T_2$  relaxation rate:

$$\Delta R_2(t) \propto C_t(t), \quad (1)$$

where  $C_t(t)$  is the contrast agent concentration in tissue at time  $t$ . This relation is a central assumption in the subsequent kinetic analysis (below).

For GE and SE sequences, signal intensity depends in an exponential fashion upon the transverse and longitudinal relaxation rates,  $R_1$  and  $R_2$ , and their rate changes,  $\Delta R_2$  and  $\Delta R_1$ , following contrast injection. Assuming that  $R_1$  remains constant (i.e., that the small enhancement due to shortening of blood  $T_1$  by the contrast agent is constant) yields the relation

$$S(t) = S(t_0)(1 - \exp^{-TR R_1}) \exp^{-TE \Delta R_2(t)}, \quad (2)$$

where  $S(t_0)$  is determined from the baseline signal in the images prior to the contrast bolus arrival, and where

$\Delta R_2$  is a function of time. Assuming the proportionality in Eq. [1], the relation between concentration and signal intensity is given by

$$C_t(t) = -k \cdot \log\left(\frac{S(t)}{S(t_0)}\right) / TE. \quad (3)$$

The assumption of linearity in Eq. [1] has been confirmed by indirect measurements *in vivo* (7) and is now widely used in perfusion measurements. In a simulation study, Kiselev and Posse (8,9) found that, due to the complex physics of MR signal formation in perfused tissues, the linearity in Eq. [3] may not hold for all ranges of contrast agent concentrations or tissues. This nonlinearity may cause overestimation of perfusion estimates (10).

## CBV MEASUREMENTS

Rosen and co-workers (11–14) derived maps of relative CBV by kinetic analysis of the concentration time curves (see above) while dynamically tracking the passage of a bolus high-susceptibility contrast agent. Note that the technique is applicable to any method of tracking the passage of an intravascular tracer with high temporal resolution, irrespective of modality (dynamic computed tomography (CT) is also suited for this purpose). The key issue is temporal resolution of the dynamic imaging relative to the characteristic blood transit time of the tissue (typically 4–6 seconds). Upon a standard 5 mL/second injection into an antecubital vein, the tissue bolus passage duration is of the order of 12–20 seconds in adults. With EPI, a typical choice of temporal resolution is  $TR = 1.5$  seconds or faster. With current high-performance gradient systems, this allows acquisition of 10–15 slices (typically with a spatial resolution of roughly 1.5 mm in plane, 5–6 mm slice thickness) for every TR, providing good brain coverage. For purposes involving deconvolution (see below), temporal resolution slower than 1.5 seconds per image is not advised.

By detecting the arterial as well as the total tissue concentration as a function of time during a single

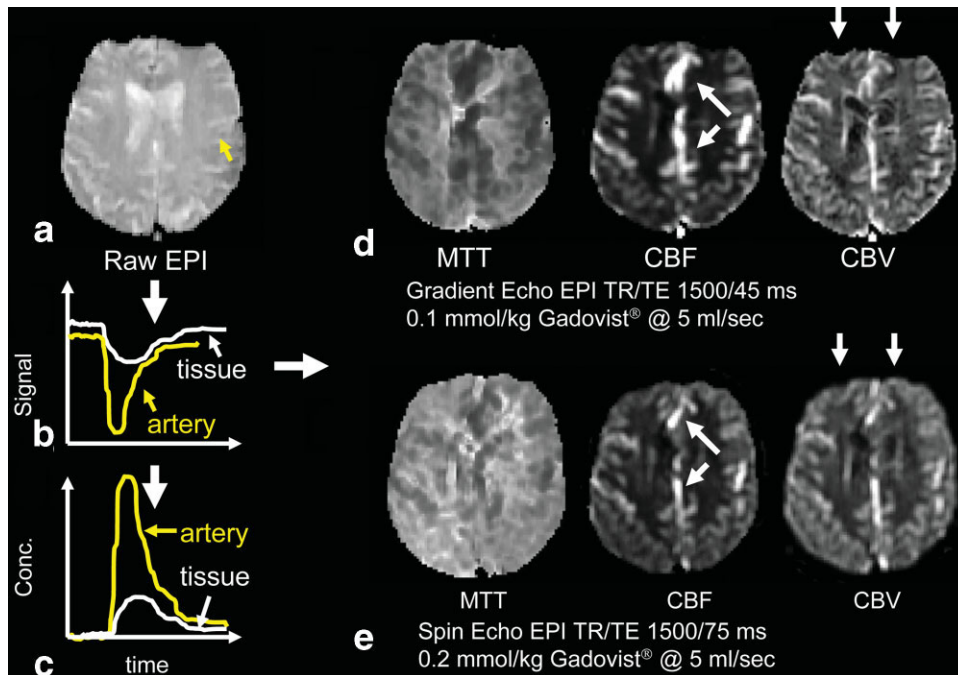


**Figure 2.** Time-course of a typical DSC imaging experiment. A contrast agent is injected into an antecubital vein while raw EPI images are acquired (a). The contrast agent reaches the brain, causing a substantial signal drop in tissue and arteries (graphed in b), which is in turn converted into contrast agent concentration (graphed in c). Based on the raw images (a), maps of CBV, CBF, and MTT are formed (d and e). CBV was determined by integration of each pixel's tissue concentration time curve and CBF by deconvolution of this curve with an AIF determined in a central slice. The GE raw images (a and d) are more prone to susceptibility artifacts near tissue-air interfaces, e.g., near the frontal sinus (vertical arrows in d) compared to the SE images (e, see vertical arrows). The microvascular sensitivity of the SE sequence makes large vessels less pronounced in the CBF maps (angled arrows in d and e). Due to the rapid bolus transit, rapid imaging is required in order to capture the first pass of the bolus, typically at a rate of one image per 1.5 seconds using FLASH or multislice EPI sequences. Rapid injection of contrast agent and saline (preferably flushed with 20 mL in adults) is imperative to obtain a sharp input bolus to the tissue. Twice the amount of contrast agent is injected for SE than for GE to compensate for the differences in sensitivity between GE and SE. For both imaging sequences, the slice thickness was 5 mm with a 1.5-mm gap. Image resolution was  $128 \times 128$  using a 240-mm field of view (FOV). TR = 1500 with TE = 75 msec for SE and TE = 45 msec for GE. A total of 48 dynamic images were recorded during the bolus passage. (Figure courtesy of Louise Gyldensted and Søren Christensen, CFIN)

transit, the CBV can be determined from the ratio of the areas under the tissue and arterial concentration time curves, respectively (15–18), as

$$\text{CBV} = \frac{\int_{-\infty}^{\infty} C_t(\tau) d\tau}{\int_{-\infty}^{\infty} C_a(\tau) d\tau}, \quad (4)$$

with concentrations determined from Eq. [3]. As arterial measurements (due to limited spatial resolution) are not readily quantifiable, relative CBV values are usually reported. Assuming uniform arterial concentration profiles in all arterial inputs, relative CBV measurements are determined by simply integrating the area under the concentration time curve (11–13), occasionally by the use of a gamma variate function to correct for tracer recirculation (19). In a recent report, Perkio et al (20) concluded that numerically integrating the area of the tissue curve (over the full time range for which it was imaged) and integrating the area of the deconvolved tissue impulse response function (see below) represent

the most accurate methods of determining relative CBV.

### THE RESIDUE FUNCTION AND CBF

The analysis of residue data (i.e., the tracer concentration in tissue after a venous injection has reached the tissue through the feeding artery) is most easily understood by first considering a simple experiment where tracer is injected directly into the feeding artery of a tissue element. To describe the tissue retention of tracer, the so-called residue function  $R(t)$  is introduced, which measures the fraction of tracer present in the vasculature at time  $t$  after injection. Accordingly, the residue is a decreasing function of time,  $R(0) = 1$ , and if the tracer is not bound to the vessels,  $R(\infty) = 0$ .

For an infinitely short lasting injection giving rise to an arterial concentration  $C_a$  at time 0, the tissue concentration  $C_t(t)$  as a function of time is

$$C_t(t) = \text{CBF} \cdot C_a \cdot R(t). \quad (5)$$

The proportionality with CBF is intuitively clear, as the concentration of contrast agent present in the tis-

sue at a given time is proportional to the amount of blood (with tracer concentration  $C_a$ ) passing through the tissue element per unit time. The product CBF  $R(t)$  is called the tissue impulse response function, as it is the tissue concentration as a result of the aforementioned impulse (infinitely short) input.

In real experiments, the arterial input function (AIF)  $C_a(t)$  is distributed in time, and the tissue concentration time curve becomes the convolution (sum of individual, very short arterial impulses above) of the tissue impulse response function and the shape of the AIF:

$$C_i(t) = \text{CBF} \cdot C_a(t) \otimes R(t). \quad (6)$$

In order to derive CBF from Eq. [6], the tissue impulse response function has to be determined by deconvolution, essentially fitting CBF  $R(t)$  from the experimental data. As  $R(0) = 1$ , CBF is determined as the initial height of the tissue impulse response function.

A number of difficulties arise when solving Eq. [6]. Because of experimental noise, the deconvolution is said to be ill-posed, meaning that wildly different solutions for the impulse response function can result in similar fits to the experimental data. The approaches to solve Eq. [6] in order to regionally determine CBF can be divided into two main categories. In model-dependent approaches, specific analytical expressions are chosen to describe the shape of  $R(t)$ . Model-dependent approaches are further discussed by L. Parkes in this issue. In the second category, model-independent approaches, deconvolution is performed in every image pixel, solving Eq. [9] for  $\text{CBF} \cdot R(t)$ . Knowledge of the specific approach chosen in a given DSC-MRI method is important in understanding some of the shortcomings of deconvolution techniques. Therefore, these approaches are shortly reviewed below.

### DETERMINING CBF AND THE RESIDUE FUNCTION USING MODEL-INDEPENDENT (DECONVOLUTION) APPROACHES

In these approaches, Eq. [6] is solved for  $\text{CBF} \cdot R(t)$  by standard mathematical deconvolution techniques, typically using a transform approach, or by a linear algebraic approach. In the Fourier transform (FT) approach, the convolution theorem of the FT is utilized, namely, that the transform of two convolved functions equals the product of their individual transforms. Hence, Eq. [6] can be solved (21,22) as

$$\begin{aligned} F\{\text{CBF} \cdot R(t) \otimes C_a(t)\} &= F\{C_i(t)\} \Rightarrow \text{CBF} \cdot R(t) \\ &= F^{-1}\left\{\frac{F\{C_i(t)\}}{F\{C_a(t)\}}\right\}, \quad (7) \end{aligned}$$

where  $F$  and  $F^{-1}$  denote the discrete and inverse discrete FTs, respectively. In the linear algebraic approach, Eq. [6] is rewritten into a matrix equation as follows (23). Assuming that tissue and arterial concentrations are measured at equidistant time points  $t_1, t_2 = t_1 + \Delta t, \dots, t_N$ , the tissue concentration  $C_i(t_j)$  at time  $t_j$  in

Eq. [6] can be reformulated as a matrix equation by noting

$$C_i(t_j) = F_t \int_0^{t_j} C_a(\tau) R(t_j - \tau) d\tau \approx F_t \Delta t \sum_{i=0}^j C_a(t_i) R(t_j - t_i) \quad (8)$$

where  $F_t$  is the tissue blood flow (i.e., the CBF). The above expression is equivalent to

$$\begin{aligned} &\begin{pmatrix} C_i(t_1) \\ C_i(t_2) \\ \vdots \\ C_i(t_N) \end{pmatrix} \\ &= F_t \cdot \Delta t \begin{pmatrix} C_a(t_1) & 0 & \dots & 0 \\ C_a(t_2) & C_a(t_1) & \dots & 0 \\ \dots & \dots & \dots & \dots \\ C_a(t_N) & C_a(t_{N-1}) & \dots & C_a(t_1) \end{pmatrix} \cdot \begin{pmatrix} R(t_1) \\ R(t_2) \\ \vdots \\ R(t_N) \end{pmatrix}, \quad (9) \end{aligned}$$

which is a standard matrix equation that can theoretically be inverted to yield CBF  $R(t)$ .

Stable solutions to Eq. [6] and Eq. [9] can only be obtained by applying techniques to suppress experimental noise. For the FT, this is achieved by applying a filter to the higher frequencies in the frequency (transformed) domain, assuming this can be done without losing physiological information. In the case of matrix equations such as Eq. [9], noise is often suppressed by regularization (forcing the solution to satisfy a priori, user-defined conditions, or otherwise be well behaved) (24) or by singular value decomposition (SVD) (23). See also Liu et al (25) for details on noise suppression by SVD.

The optimal choice of some transform and linear algebraic approaches was studied by Østergaard et al (26) using Monte Carlo simulations. It was found that the FT approach has an inherent problem in arriving at true CBF due to the discontinuity of the tissue impulse response function at  $t = 0$  (FTs are optimal for smooth functions). In a subsequent analysis by Alsop and Schlaug (27), the SVD and FT methods were shown to be equivalent when certain periodicity criteria are met. This may explain the findings of Smith et al (28), who found SVD and FT to yield similar CBF values only when tissue concentration curves were first fitted to a gamma variate function. Further evidence suggests that, in normal volunteers, the FT dependence upon vascular structure does not lead to appreciable differences in relative CBF estimates from those obtained by the SVD approach (29). The FT approach has the attraction of theoretically being insensitive to delays between the AIF and the tissue, as may be observed in cerebrovascular disease.

Of the linear algebraic approaches, regularization showed an inherent dependency on signal-to-noise ratio (and thereby regional blood volume). Deconvolution by SVD, however, showed a remarkable independence upon vascular structure and CBV, yielding reasonably accurate CBF estimates even at the signal-to-noise ra-

tio of pixel-by-pixel calculations used in clinical EPI measurements. The major disadvantage of the original SVD approach is a tendency to underestimate flow when tissue tracer arrival is delayed relative to the AIF (26,30,31). This problem has been circumvented by the so-called circular SVD, recently published by Wu et al (32).

### MODEL-DEPENDENT APPROACH

The model-independent deconvolution techniques described above make no assumptions regarding the vascular structure. Also, in principle the model-independent approaches enable the regional vascular transit time characteristics to be determined along with tissue flow by studying the residue function. As an alternative, the model-dependent approaches below model tracer transport and retention, and must therefore be chosen very carefully in order not to lose generality and thereby bias the resulting flow values. Larson et al (33) suggested an exponential residue model, assuming the microvasculature to behave like a single, well-mixed compartment. Although residue functions determined by model-less approaches often appear exponential, this model tends to bias resulting flow values in cases where the underlying residue function is nonexponential (26). Østergaard et al (34) modified and applied a model of macrovascular transport and microvascular retention in the brain. The model, originally introduced to describe tracer transport and retention in the heart (35,36), utilizes vascular transport operators, allowing detailed modeling of the delay and dispersion of the arterial input due to the passage through the artery downstream of the measurement site.

### STATISTICAL APPROACHES

Vonken et al (37,38) suggested a statistical approach, optimizing the kernel (residue function in Eq. [9]) by a maximum likelihood approach, with the further advantage of allowing for delayed tracer arrival relative to the measured arterial input. In another statistical approach, Andersen et al (39) used a Gaussian process technique to approximate the convolution kernel. Although overly computationally demanding, this represents a promising approach to studying the residue function.

Whereas the model-less approaches offer simultaneous determination of flow and vascular residue function, the vascular model approach requires a model of major vessel transport as well as microvascular retention. Major vessel dispersion and microvascular retention can then to some extent be distinguished, stabilizing CBF estimates. On the other hand, abnormal capillary perfusion patterns (and thereby deviation from the normal flow heterogeneity) are likely to affect flow estimates by these model-dependent approaches (40,41).

### THE MTT

As pointed out by Weisskoff et al (41), the distinction between MTT and the first moment of the tissue con-

centration time curve is crucial in attempts to measure transit times using intravascular tracers. The calculation of MTT thereby requires knowledge of the transport function or CBF, as by the central volume theorem (15),

$$MTT = \frac{CBV}{F_t}. \quad (10)$$

### QUANTIFICATION

The formalism above produces absolute values for CBF and CBV provided arterial and tissue concentrations are experimentally determined in identical units. This, however, represents a number of practical problems in actual clinical applications. Due to the inherently limited spatial resolution of MRI relative to vessel sizes, absolute arterial tracer concentration measurements are difficult to obtain from image data. Several studies have applied Fast Low Angle Shot (FLASH)-type imaging sequences, allowing measurements of arterial levels in a separate, low slice with a short echo time, hence avoiding complete loss of vascular signal during the bolus passage (21,37). These studies yielded somewhat high absolute CBF, possibly due to the choice of deconvolution approach, or due to partial volume and averaging effects. In a recent study by Schreiber et al (42), absolute values in good agreement with accepted flow rates were obtained. In multislice EPI experiments, a single echo is generally used, optimizing tissue signal loss, thereby often causing complete signal loss at major vessels. Therefore, smaller arterial branches having partial volume effects with surrounding tissue are used, and consequently, the shape rather than the absolute amplitude of the AIF is obtained in these experiments. Intersubject comparisons must therefore be performed using internal references believed to have little intersubject variability, for example, white matter or cerebellum. In an attempt to obtain absolute flow values from EPI experiments, Østergaard et al assumed proportionality between the area of the AIF and the injected contrast dose, using water clearance PET as a calibration method. This approach provided reproducible absolute CBF measurements in animal hypercapnia studies (6) and in humans (43). However, this approach may be too crude to allow general use in patients with severe cardiac or cerebrovascular disease.

### DELAY AND DISPERSION

Even though a straightforward delay of tracer arrival can be accounted for by methods such as circular SVD, model-less approaches cannot distinguish tracer dispersion in feeding vessels from tracer retention in the capillary bed. Specifically, a large degree of vessel dispersion will be interpreted as a low flow, although actual tissue flow may be normal (26,31). This is a more fundamental limitation that cannot be circumvented unless a specific model of major vessel dispersion is assumed (e.g., by a vascular operator, as in Østergaard et al (34)).

Utilizing the spatial resolution of the raw perfusion images, Alsop et al (44) suggested detecting AIF region-

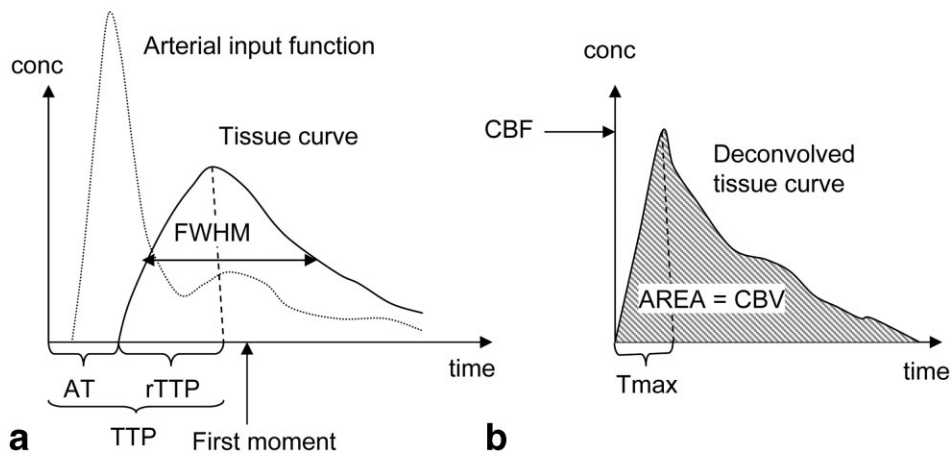


**Figure 3. a:** The measured tissue concentration time curve (tissue curve) gives rise to various measures of the transit time that all depend on the local shape of the AIF. The arrival time (AT) of the bolus mainly reflects collateral circulation. The time to peak, to some extent, reflects tissue transit time (rTTP) and, if arrival delay is included, also reflects collateral circulation (TTP). The first moment (the center of gravity) and the full width at half maximum (FWHM) of the tissue concentration time curve mainly depend on tissue MTT. **b:** Deconvolution of the curves in (a) removes the dependence on the arterial input curve and produces the deconvolved tissue curve. In the presence of arterial delays, the deconvolved curve is not maximal at  $t = 0$ , but instead is maximal (the tissue impulse response function) after a certain delay (Tmax). CBF is usually taken as the curve height of the deconvolved curve at time Tmax. MTT is calculated as  $CBV/CBF$ , where CBV is determined as the area under the deconvolved curve (b) or the tissue curve (a). However, calculation of CBV from the tissue curve requires laborious corrections for tracer recirculation.

ally, i.e., from arterial branches close to the tissue voxel being analyzed. Although correctly assigning the arterial supply of a voxel to one of several nearby arterial branches may be difficult, e.g., in vascular watershed areas and in vascular occlusion (stroke), this may prove a promising approach in overcoming the inherent methodological problem of dispersion.

### FLOW HETEROGENEITY AND METABOLIC SIGNIFICANCE OF THE RESIDUE FUNCTION

As diffusible solutes such as oxygen pass through the capillary bed, they are extracted by the tissue. The extraction fraction (fraction of substance extracted during a single pass) of a solute is given by (45,46)

$$E = (1 - e^{-\frac{PS}{F_t}}), \quad (11)$$

where  $P$  is the permeability and  $S$  the surface area of the capillary endothelium. Note that for  $F_t \ll PS$ , extraction is near unity, whereas when flow approaches or exceeds  $PS$ , extraction becomes incomplete. For a system of capillaries with identical  $PS$  and with a distribution of relative flows  $w(f)$ , the extraction fraction therefore becomes

$$E = \int_0^{\infty} w(f) (1 - e^{-\frac{PS}{fF_t}}) df, \quad (12)$$

where  $w(f)$  is the probability density function (PDF) describing the flow distribution. Assuming the  $PS$  product for a given molecule and tissue is essentially constant, the flow and associated flow heterogeneity become the prime determinants of solute extraction when  $PS$  is

large (i.e., extraction is determined by flow rather than permeability). In particular, if flow is fixed (e.g., in acute stroke), extraction can only be modified by altering flow heterogeneity.

The residue function and the flow distribution PDF  $w(f)$  are related through the distribution of transit times,  $h(t)$ , also called the transport function. The transport function is the slope of the residue function given by

$$h(t) = -\frac{dR}{dt}, \quad (13)$$

and the distribution of flows is given by

$$w(f) = -\frac{T}{f} \cdot h(T), \quad (14)$$

where  $f$  is the relative flow and  $T$  is the transit time ( $CBV/F_t$ ). Combining Eq. [14] and Eq. [13] therefore yields flow heterogeneity in terms of the residue function. Flow heterogeneity, in turn, determines the extraction fraction by Eq. [12].

### OTHER HEMODYNAMIC INDICES

The derivation of flow and transit time from bolus tracking requires measurement of arterial input tracer levels. In some cases, this measurement may not be practical, just as the inherent complexity of deconvolution approaches may preclude the use of those techniques in some situations. Indices derivable directly from the tissue concentration time curves (dark line in Fig. 3a) involve time to peak (the time from injection to when the maximum concentration is reached), arrival time (ar-

rival time of tracer in the pixel), full width at half maximum of the tissue curve shape, and first moment of the tissue curve. Based on the deconvolved tissue curve (Fig. 3b), a delay of the occurrence of the peak value (the height of the curve, defining CBF) can be defined, sometimes referred to as  $T_{\max}$  (47). Although the dependence of these indices on MTT and CBF depends strongly on the vascular structure and the AIF (41), these indices often suffice to delineate pathological changes and provide important qualitative information in many diseases. It appears, however, that the derivation of CBF, CBV, and MTT from kinetic principles somewhat improves specificity and sensitivity of clinical studies, facilitating inter- and intrasubject comparisons (48).

## CONCLUSION

The principles of DSC-MRI cerebral perfusion imaging (bolus tracking) have been described and reviewed. Several numerical methods exist for measuring CBF depending on the numerical method that is used. Methods that measure the residue function also could assess flow heterogeneity, in principle. Other hemodynamic indices can be measured from the tissue curve.

## REFERENCES

- Calamante F, Thomas DL, Pell GS, Wiersma J, Turner R. Measuring cerebral blood flow using magnetic resonance imaging techniques. *J Cereb Blood Flow Metab* 1999;19:701-735.
- Villringer A, Rosen BR, Belliveau JW, et al. Dynamic imaging with lanthanide chelates in normal brain: contrast due to magnetic susceptibility effects. *Magn Reson Med* 1988;6:164-174.
- Fisel CR, Ackerman JL, Buxton RB, et al. MR contrast due to microscopically heterogeneous magnetic susceptibility: numerical simulations and applications to cerebral physiology. *Magn Reson Med* 1991;17:336-347.
- Boxerman JL, Hamberg LM, Rosen BR, Weisskoff RM. MR contrast due to intravascular magnetic susceptibility perturbations. *Magn Reson Med* 1995;34:555-566.
- Weisskoff RM, Zuo CS, Boxerman JL, Rosen BR. Microscopic susceptibility variation and transverse relaxation: theory and experiment. *Magn Reson Med* 1994;31:601-610.
- Østergaard L, Smith DF, Vestergaard-Poulsen P, et al. Absolute cerebral blood flow and blood volume measured by magnetic resonance imaging bolus tracking: comparison with positron emission tomography values. *J Cereb Blood Flow Metab* 1998;18:425-432.
- Simonsen CZ, Østergaard L, Vestergaard-Poulsen P, Rohl L, Bjørnerud A, Gyldensted C. CBF and CBV measurements by USPIO bolus tracking: reproducibility and comparison with Gd-based values. *J Magn Reson Imaging* 1999;9:342-347.
- Kiselev VG, Posse S. Analytical theory of susceptibility induced NMR signal dephasing in a cerebrovascular network. *Phys Rev Lett* 1998;81:5696-5699.
- Kiselev VG, Posse S. Analytical model of susceptibility-induced MR signal dephasing: effect of diffusion in a microvascular network. *Magn Reson Med* 1999;41:499-509.
- Kiselev VG. On the theoretical basis of perfusion measurements by dynamic susceptibility contrast MRI. *Magn Reson Med* 2001;46:1113-1122.
- Rosen BR, Belliveau JW, Vevea JM, Brady TJ. Perfusion imaging with NMR contrast agents. *Magn Reson Med* 1990;14:249-265.
- Rosen BR, Belliveau JW, Aronson HJ, et al. Susceptibility contrast imaging of cerebral blood volume: human experience. *Magn Reson Med* 1991;22:293-299; see discussion, pp. 300-293.
- Rosen BR, Belliveau JW, Buchbinder BR, et al. Contrast agents and cerebral hemodynamics. *Magn Reson Med* 1991;19:285-292.
- Belliveau JW, Kennedy Jr DN, McKinstry RC, et al. Functional mapping of the human visual cortex by magnetic resonance imaging. *Science* 1991;254:716-719.
- Stewart GN. Researches on the circulation time in organs and on the influences which affect it. Parts I-III. *J Physiol (London)* 1894;15:1-89.
- Meier P, Zierler KL. On the theory of the indicator-dilution method for measurement of blood flow and volume. *J Appl Physiol* 1954;6:731-744.
- Zierler KL. Equations for measuring blood flow by external monitoring of radioisotopes. *Circ Res* 1965;16:309-321.
- Zierler KL. Theoretical basis of indicator-dilution methods for measuring flow and volume. *Circ Res* 1962;10:393-407.
- Thompson Jr HK, Starmer CF, Whalen RE, McIntosh HD. Indicator transit time considered as a gamma variate. *Circ Res* 1964;14:502-515.
- Perkio J, Aronson HJ, Kangasmaki A, et al. Evaluation of four post-processing methods for determination of cerebral blood volume and mean transit time by dynamic susceptibility contrast imaging. *Magn Reson Med* 2002;47:973-981.
- Rempp KA, Brix G, Wenz F, Becker CR, Guckel F, Lorenz WJ. Quantification of regional cerebral blood flow and volume with dynamic susceptibility contrast-enhanced MR imaging. *Radiology* 1994;193:637-641.
- Gobbel GT, Fike JR. A deconvolution method for evaluating indicator-dilution curves. *Phys Med Biol* 1994;39:1833-1854.
- Van Huffel S, Vandewalle J, De Roo MC, Willems JL. Reliable and efficient deconvolution technique based on total linear least squares for calculating the renal retention function. *Med Biol Eng Comput* 1987;25:26-33.
- Bronikowski TA, Dawson CA, Linehan JH. Model-free deconvolution techniques for estimating vascular transport functions. *Int J Biomed Comput* 1983;14:411-429.
- Liu HL, Pu Y, Liu Y, et al. Cerebral blood flow measurement by dynamic contrast MRI using singular value decomposition with an adaptive threshold. *Magn Reson Med* 1999;42:167-172.
- Østergaard L, Weisskoff RM, Chesler DA, Gyldensted C, Rosen BR. High resolution measurement of cerebral blood flow using intravascular tracer bolus passages. Part I. Mathematical approach and statistical analysis. *Magn Reson Med* 1996;36:715-725.
- Alsop D, Schlaug G. The equivalence of SVD and Fourier deconvolution for dynamic susceptibility contrast analysis. In: Proceedings of the 9th Annual Meeting of ISMRM, Glasgow, Scotland, 2001. p 1581.
- Smith AM, Grandin CB, Duprez T, Mataigne F, Cosnard G. Whole brain quantitative CBF, CBV, and MTT measurements using MRI bolus tracking: implementation and application to data acquired from hyperacute stroke patients. *J Magn Reson Imaging* 2000;12:400-410.
- Wirestam R, Andersson L, Østergaard L, et al. Assessment of regional cerebral blood flow by dynamic susceptibility contrast MRI using different deconvolution techniques. *Magn Reson Med* 2000;43:691-700.
- Wu O, Østergaard L, Koroshetz WJ, et al. Effects of tracer arrival time on flow estimates in MR perfusion-weighted imaging. *Magn Reson Med* 2003;50:856-864.
- Calamante F, Gadian DG, Connolly A. Delay and dispersion effects in dynamic susceptibility contrast MRI: simulations using singular value decomposition. *Magn Reson Med* 2000;44:466-473.
- Wu O, Østergaard L, Weisskoff RM, Benner T, Rosen BR, Sorensen AG. Tracer arrival timing-insensitive technique for estimating flow in MR perfusion-weighted imaging using singular value decomposition with a block-circulant deconvolution matrix. *Magn Reson Med* 2003;50:164-174.
- Larson KB, Perman WH, Perlmutter JS, Gado MH, Ollinger JM, Zierler K. Tracer-kinetic analysis for measuring regional cerebral blood flow by dynamic nuclear magnetic resonance imaging. *J Theor Biol* 1994;170:1-14.
- Østergaard L, Chesler DA, Weisskoff RM, Sorensen AG, Rosen BR. Modeling cerebral blood flow and flow heterogeneity from magnetic resonance residue data. *J Cereb Blood Flow Metab* 1999;19:690-699.
- King RB, Deussen A, Raymond GM, Bassingthwaite JB. A vascular transport operator. *Am J Physiol* 1993;265:H2196-H2208.
- King RB, Raymond GM, Bassingthwaite JB. Modeling blood flow heterogeneity. *Ann Biomed Eng* 1996;24:352-372.
- Vonken EJ, van Osch MJ, Bakker CJ, Viergever MA. Measurement of cerebral perfusion with dual-echo multi-slice quantitative dynamic susceptibility contrast MRI. *J Magn Reson Imaging* 1999;10:109-117.

38. Vonken EP, Beekman FJ, Bakker CJ, Viergever MA. Maximum likelihood estimation of cerebral blood flow in dynamic susceptibility contrast MRI. *Magn Reson Med* 1999;41:343-350.
39. Andersen IK, Szymkowiak A, Rasmussen CE, et al. Perfusion quantification using Gaussian process deconvolution. *Magn Reson Med* 2002;48:351-361.
40. Lassen NA. Cerebral transit of an intravascular tracer may allow measurement of regional blood volume but not regional blood flow. *J Cereb Blood Flow Metab* 1984;4:633-634.
41. Weisskoff RM, Chesler D, Boxerman JL, Rosen BR. Pitfalls in MR measurement of tissue blood flow with intravascular tracers: which mean transit time? *Magn Reson Med* 1993;29:553-558.
42. Schreiber WG, Guckel F, Stritzke P, Schmiedek P, Schwartz A, Brix G. Cerebral blood flow and cerebrovascular reserve capacity: estimation by dynamic magnetic resonance imaging. *J Cereb Blood Flow Metab* 1998;18:1143-1156.
43. Østergaard L, Johannsen P, Host-Poulsen P, et al. Cerebral blood flow measurements by magnetic resonance imaging bolus tracking: comparison with [(15)O]H<sub>2</sub>O positron emission tomography in humans. *J Cereb Blood Flow Metab* 1998;18:935-940.
44. Alsop DC, Wedmid A, Schlaug G. Defining a local input function for perfusion quantification with bolus contrast MRI. In: *Proceedings of the 10th Annual Meeting of ISMRM, Honolulu, 2002.* p 659.
45. Crone C. The permeability of capillaries in various organs as determined by use of the 'indicator diffusion' method. *Acta Physiol Scand* 1963;58:292-305.
46. Renkin EM. Exchangeability of tissue potassium in skeletal muscle. *Am J Physiol* 1959;197:1211-1215.
47. Shih LC, Saver JL, Alger JR, et al. Perfusion-weighted magnetic resonance imaging thresholds identifying core, irreversibly infarcted tissue. *Stroke* 2003;34:1425-1430.
48. Yamada K, Wu O, Gonzalez RG, et al. Magnetic resonance perfusion-weighted imaging of acute cerebral infarction: effect of the calculation methods and underlying vasculopathy. *Stroke* 2002;33:87-94.